

# Pseudo-Fourier modal analysis of two-dimensional arbitrarily shaped grating structures

Hwi Kim and Byoung-ho Lee\*

*National Creative Research Center for Active Plasmonics Applications Systems, Inter-University Semiconductor Research Center and School of Electrical Engineering, Seoul National University, Gwanak-Gu Sinlim-Dong, Seoul 151-744, Korea*

\*Corresponding author: byoung-ho@snu.ac.kr

Received July 17, 2007; revised October 4, 2007; accepted October 8, 2007;  
posted October 15, 2007 (Doc. ID 85322); published December 5, 2007

The pseudo-Fourier modal analysis of two-dimensional arbitrarily shaped grating structures is described. It is shown that the pseudo-Fourier modal analysis has an advantage of improved structure modeling over the conventional rigorous coupled-wave analysis. In the conventional rigorous coupled-wave analysis, grating structures are modeled by the staircase approximation, which is well known to have inherent significant errors under TM polarization. However, in the pseudo-Fourier modal analysis, such a limitation of the staircase approximation can be overcome through the smooth-structure modeling based on two-dimensional Fourier representation. The validity of the claim is proved with some comparative numerical results from the proposed pseudo-Fourier modal analysis and the conventional rigorous coupled-wave analysis. © 2007 Optical Society of America

OCIS codes: 000.3860, 000.6800, 050.1960, 050.1950, 050.0050, 050.1940.

## 1. INTRODUCTION

During the past few decades, Fourier modal methods (FMMs) [1–5] have been intensively researched, and many challenging difficulties related to the fundamentals of the FMM have been overcome. At present, the FMM is well established and is considered to be one of the most efficient and accurate tools for electromagnetic analysis in optics and photonics. Among recent advances in the FMM, Li's Fourier factorization rule [3–5], the fast Fourier factorization rule by Popov and Nevière [6,7] for proper convergence in transverse magnetic (TM) polarization, perfectly matched layers (PMLs) [8], the scattering matrix ( $S$ -matrix) method (SMM) [9,10], and the validation examination of the staircase approximation [11] are particularly notable.

The limitation of the staircase approximation and its resolution were discussed in the framework of the differential theory [11]. In the conventional rigorous coupled-wave analysis (RCWA), the structures indicated by the permittivity and permeability functions are usually staircase-approximated along the longitudinal direction, and then the main field equation takes the form of a coupled differential equation system with constant coefficients at each layer. In the differential theory, the main differential equation system with nonconstant coefficients derived from the Maxwell equations is solved by the numerical integration technique. In [11], it is shown that the staircase approximation adopted in the RCWA can produce significant errors in the field distribution, particularly within metallic gratings, and the differential theory without the staircase approximation can reduce the errors.

Recently, some spectral-(frequency)-domain-analysis-based studies on the Maxwell equations with nonconstant

coefficients without the staircase approximation were reported [12–16]. In the FMM-based studies [12,13], by adopting full-Fourier representation of the structures and fields without the staircase approximation, the differential equation system with nonconstant coefficients is transformed to an algebraic eigenvalue equation in the Fourier domain (spatial-frequency domain). In [14–16], fields and structures are represented by Legendre polynomial expansion. In this case, also, longitudinally inhomogeneous structures are analyzed without the staircase approximation.

Henceforth we name the FMM-based full-frequency method the pseudo-Fourier modal analysis (PFMA) method following the naming used in our previous paper [13]. The PFMA is a mathematical generalization of the RCWA. In the PFMA, a complete Fourier analysis is applied to the coupled nonconstant differential equation system. For performing this task, in the PFMA, electromagnetic fields and structures are represented by the pseudo-Fourier series and the Fourier series, respectively. From the viewpoint of mathematical modeling, the most noteworthy feature of the PFMA may be the nonuse of the staircase approximation.

Interestingly, the key idea and mathematics of the PFMA were reported independently by Jiang and Chen [12] and Kim and Lee [13] at almost the same time. In [13], the PFMA on a one-dimensional (1-D) structure is formulated and the convergence of the PFMA is analyzed. However, in [12], an extension of the method using the concept of "virtual photonic crystal" for analyzing two-dimensional (2-D) grating structures is described, which is actually equivalent to 2-D PFMA for single-layer grating structures.

In this paper, an extension and refinement of the 2-D

PFMA addressed in [12] is presented. The most important feature in the described PFMA is the combination of the PFMA and the extended  $S$ -matrix method (ESMM) [10] for analyzing deep continuous grating structures. The PFMA is applied for characterizing the  $S$  matrix of a single layer of a multilayer. The obtained  $S$  matrices of the constituent layers are manipulated to form the total  $S$  matrix of the whole multilayer structure according to Redheffer's star product rule of the SMM.

As a result, within the framework, structures—in particular, deep continuous grating structures—are modeled by smooth and continuous multilayer structures. The nonuse of the staircase approximation in the proposed PFMA scheme may lead to proper field distribution calculations for deep continuous metallic grating structures that cannot be obtained by the conventional RCWA scheme with the staircase approximation. The validity of our claim is proved with some numerical results comparing the proposed PFMA and the conventional RCWA.

The paper is organized as follows. In Section 2, the general 2-D scheme of the PFMA is described. In Section 3, the multilayer structure analysis with the ESMM is presented. In Section 4, numerical results for comparing the RCWA and the proposed PFMA are presented and discussed. In Section 5, concluding remarks are given.

## 2. PSEUDO-FOURIER MODAL ANALYSIS

The basic concepts and 1-D implementation of the PFMA have been established in [13]. In this section, the 2-D version of the previous 1-D PFMA is described. As previously stated, a similar 2-D formulation has been already reported by Jiang and Chen [12]. However, we give a refined formulation concerning the combination of the PFMA and the ESMM. It will be interesting to compare our formulation and that of [12]. For convenience, the same notations and frameworks as used in [13] are used in the description of the theory. Vectors and matrices are underlined and double-underlined, respectively. The time-varying term is assumed to be  $\exp(-j\omega t)$ . A grating structure with finite width along the  $z$  direction is located in the  $x$ - $y$  plane as shown in Fig. 1; this is usually modeled by a multilayer structure. The thickness and the period of the grating are denoted by  $d$  and  $\Lambda_x$ , respectively. In region I, a plane wave  $\underline{E}_{inc}$  is incident to the grating structure, and the corresponding reflection field  $\underline{E}_R$  and transmission field  $\underline{E}_T$  are generated in regions I and II, respectively. The calculation and visualization of the vector field distribution in the grating region as well as in regions I and II are the main tasks of the PFMA.

First, the structure modeling in the PFMA and the RCWA are compared. In the RCWA, the grating structure shown in Fig. 2(a) is modeled with the staircase approximation as shown in Fig. 2(b), while in the PFMA, it is modeled with the continuous and smooth multilayer model as shown in Fig. 2(c). Therefore, in the RCWA, the permittivity and permeability profiles,  $\varepsilon^{(n)}(x)$  and  $\mu^{(n)}(x)$ , of the  $n$ th layer are expressed, respectively, by 1-D Fourier series as

$$\varepsilon^{(n)}(x) = \sum_g \tilde{\varepsilon}_g^{(n)} \exp(jG_{x,g}x), \quad (1a)$$

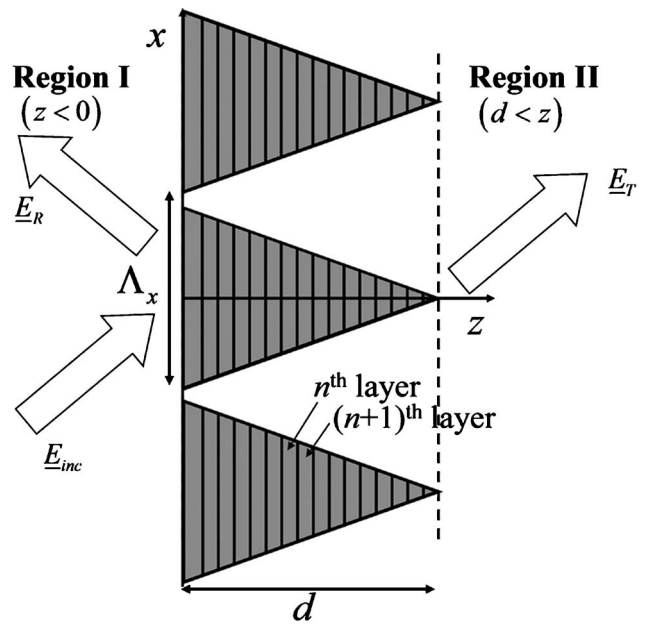


Fig. 1. Multilayer modeling of the grating to be analyzed.

$$\mu^{(n)}(x) = \sum_g \tilde{\mu}_g^{(n)} \exp(jG_{x,g}x), \quad (1b)$$

where  $G_{x,g}$  is the  $x$ -direction reciprocal vector component defined by  $G_{x,g} = (2\pi/\Lambda_x)g$ . In the PFMA, as shown in Fig. 2(c), the grating structure is modeled by a smoothly connected multilayer structure. The  $n$ th layer is described by the Fourier representation of the permittivity and the permeability profiles as

$$\hat{\varepsilon}^{(n)}(x,z) = \sum_{g,h} \tilde{\varepsilon}_{gh}^{(n)} \exp[j(G_{x,g}x + G_{z,h}z)], \quad (2a)$$

$$\hat{\mu}^{(n)}(x,z) = \sum_{g,h} \tilde{\mu}_{gh}^{(n)} \exp[j(G_{x,g}x + G_{z,h}z)], \quad (2b)$$

where  $G_{z,h}$  is the  $z$ -direction reciprocal vector component defined by  $G_{z,h} = (2\pi/\Delta d)h$  and  $\Delta d$  is the thickness of a single layer.  $\hat{\varepsilon}^{(n)}(x,z)$  and  $\hat{\mu}^{(n)}(x,z)$  are the periodic extension [13] (i.e., longitudinal supercell) of the permittivity profile  $\varepsilon^{(n)}(x,z)$  and the permeability profile  $\mu^{(n)}(x,z)$  defined, respectively, by

$$\hat{\varepsilon}^{(n)}(x,z) = \varepsilon^{(n)}(x,z) \otimes \sum_{q=-\infty}^{\infty} \delta(z - q\Delta d), \quad (2c)$$

$$\hat{\mu}^{(n)}(x,z) = \mu^{(n)}(x,z) \otimes \sum_{q=-\infty}^{\infty} \delta(z - q\Delta d). \quad (2d)$$

In addition, let the reciprocal permittivity and permeability profiles  $\hat{\alpha}^{(n)}(x,z)$  and  $\hat{\beta}^{(n)}(x,z)$  be defined as, for use in the latter part of the paper,

$$\hat{\alpha}^{(n)}(x,z) = \frac{1}{\hat{\varepsilon}^{(n)}(x,z)} = \sum_{g,h} \tilde{\alpha}_{gh}^{(n)} \exp[j(G_{x,g}x + G_{z,h}z)], \quad (2e)$$

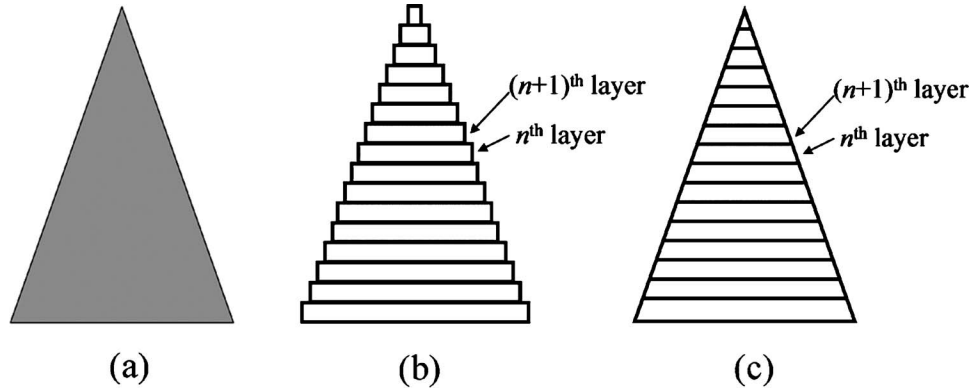


Fig. 2. (a) Target grating structure, (b) structure modeling in the RCWA, (c) structure modeling in the PFMA.

$$\hat{\beta}^{(n)}(x,z) = \frac{1}{\hat{\mu}^{(n)}(x,z)} = \sum_{g,h} \tilde{\beta}_{gh}^{(n)} \exp[j(G_{x,g}x + G_{z,h}z)]. \quad (2f)$$

The analysis of the multilayer structures is conducted with the ESMM. In the ESMM described in Section 3, to obtain the total analysis of a multilayer structure, complete electromagnetic characterization of each single layer composing the multilayer must be done first. Since the details of the ESMM will be described in the next section, in this section the PFMA on a single layer, the  $n$ th layer of the multilayer structure placed in free space shown in Fig. 1, is elucidated.

Let the  $n$ th layer be put in free space as shown in Fig. 3, where region I and region II indicate left-hand half-infinite free space and right-hand half-infinite free space, respectively. An incident plane wave  $\underline{E}_{inc}$  impinges on the single layer, and then the reflection field  $\underline{E}_R$  and the transmission field  $\underline{E}_T$  are generated in regions I and II, respectively. In the 2-D PFMA, electromagnetic fields are represented by 2-D pseudo-Fourier series. In regions I and II, the electric field distributions are expressed, respectively, by the superposition of the incident wave  $\underline{E}_{inc}$  and the reflection field  $\underline{E}_R$ , and the transmission field  $\underline{E}_T$ ,

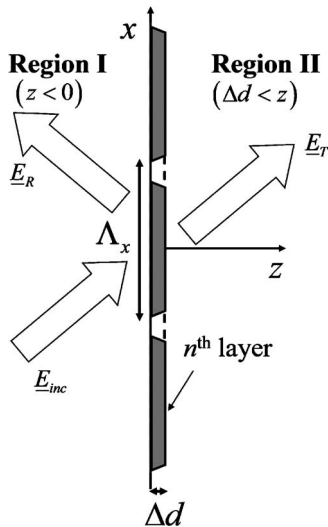


Fig. 3. Analysis of a single layer.

$$\underline{E}_I = \underline{E}_{inc} + \underline{E}_R = \underline{E}_{inc} + \sum_{h=-H}^H (r_{x,h}\hat{x} + r_{y,h}\hat{y} + r_{z,h}\hat{z}) \times \exp[j(k_{x,h}x + k_{y,y} - k_{I,z,h}z)], \quad (3a)$$

$$\underline{E}_{II} = \underline{E}_T = \sum_{h=-H}^H (t_{x,h}\hat{x} + t_{y,h}\hat{y} + t_{z,h}\hat{z}) \times \exp[j(k_{x,h}x + k_{y,y} + k_{II,z,h}(z - \Delta d))], \quad (3b)$$

where the incidence plane wave  $\underline{E}_{inc}$  is given by

$$\underline{E}_{inc} = \underline{E}_0(u_{x,s}\hat{x} + u_{y,s}\hat{y} + u_{z,s}\hat{z}) \exp[j(k_{x,s}x + k_{y,y} + k_{I,z,s}z)]. \quad (3c)$$

Here,  $k_{x,s}$  and  $k_{I,z,s}$  are the  $x$ - and  $z$ -direction wavevector components of the  $s$ th order diffraction channel in region I, which are defined, respectively, by

$$k_{x,s} = k_{x,0} + G_{x,s}, \quad \text{for } -H \leq s \leq H, \quad (4a)$$

$$k_{I,z,s} = \sqrt{(k_0 n_I)^2 - (k_{x,s})^2 - (k_y)^2}, \quad (4b)$$

and  $k_{II,z,h}$  is the  $z$ -direction wavevector component of the  $h$ th order diffraction channel in region II, which is defined by

$$k_{II,z,s} = \sqrt{(k_0 n_{II})^2 - (k_{x,h})^2 - (k_y)^2}, \quad (4c)$$

where  $k_{x,0}$  and  $k_y$  are the wavevector components of the 0th diffraction channel given, respectively, by

$$k_{x,0} = k_0 n_I \sin \theta \cos \phi, \quad (4d)$$

$$k_y = k_0 n_I \sin \theta \sin \phi, \quad (4e)$$

where  $\theta$ ,  $\phi$ , and  $\psi$  indicate the incidence angle, the azimuthal angle, and the polarization angle of the 0th diffraction channel, and  $k_0$ ,  $n_I$ , and  $n_{II}$  are the free-space wavenumbers given by  $2\pi/\lambda$  and the refractive indices of regions I and II, respectively.

In the grating region, the electromagnetic fields are represented by the superposition of Bloch eigenmodes of the grating structure. From Bloch's theorem, the Bloch eigenmodes of the electric and magnetic fields  $\underline{E}_k$  and  $\underline{H}_k$  inside the grating structure are, respectively, given by

$$\underline{E}_k = \exp[j(k_{x,0}x + k_y y + k_{z,0}z)]\hat{E}_k(x,y,z), \quad (5a)$$

$$\underline{H}_k = \exp[j(k_{x,0}x + k_y y + k_{z,0}z)]\hat{H}_k(x,y,z), \quad (5b)$$

where  $k_{z,0}$  is the eigenvalue characterizing the eigenmode pair  $\underline{E}_k$  and  $\underline{H}_k$ ,  $\underline{k}$  denotes the wavevector given by  $\underline{k} = (k_{x,0}, k_y, k_{z,0})$ , and  $\hat{E}_k(x,y,z)$  and  $\hat{H}_k(x,y,z)$  are the periodic envelope functions of electric and magnetic fields, respectively. Furthermore, the Bloch eigenmodes  $\underline{E}_k$  and  $\underline{H}_k$  are represented by the pseudo-Fourier representations:

$$\begin{aligned} \underline{E}_k &= E_{x,0} + E_{y,0} + E_{z,0} \\ &= \exp(j(k_{x,0}x + k_y y + k_{z,0}z))\underline{E}_k \\ &= \exp(j(k_{x,0}x + k_y y + k_{z,0}z)) \sum_{h=-H}^H \sum_{q=-Q}^Q (E_{x,h,q} \underline{x} \\ &\quad + E_{y,h,q} \underline{y} + E_{z,h,q} \underline{z}) \exp(j(G_{x,h}x + G_{z,q}z)), \end{aligned} \quad (6a)$$

$$\begin{aligned} \underline{H}_k &= H_{x,0} + H_{y,0} + H_{z,0} \\ &= \exp(j(k_{x,0}x + k_y y + k_{z,0}z))\underline{H}_k(x,y,z) \\ &= \exp(j(k_{x,0}x + k_y y + k_{z,0}z))j \sqrt{\frac{\epsilon_0}{\mu_0}} \sum_{h=-H}^H \sum_{q=-Q}^Q (H_{x,h,q} \underline{x} \\ &\quad + H_{y,h,q} \underline{y} + H_{z,h,q} \underline{z}) \exp(j(G_{x,h}x + G_{z,q}z)). \end{aligned} \quad (6b)$$

The Maxwell equations with the permittivity profile  $\epsilon(x,z)$  and permeability profile  $\mu(x,z)$  are given by

$$\begin{aligned} \nabla \times \underline{E} &= (\partial_y E_z - \partial_z E_y) \underline{x} + (\partial_z E_x - \partial_x E_z) \underline{y} + (\partial_x E_y - \partial_y E_x) \underline{z} \\ &= j\omega\mu_0\mu(x,z)(H_x \underline{x} + H_y \underline{y} + H_z \underline{z}), \end{aligned} \quad (7a)$$

$$\begin{aligned} \nabla \times \underline{H} &= (\partial_y H_z - \partial_z H_y) \underline{x} + (\partial_z H_x - \partial_x H_z) \underline{y} + (\partial_x H_y - \partial_y H_x) \underline{z} \\ &= -j\omega\epsilon_0\epsilon(x,z)(E_x \underline{x} + E_y \underline{y} + E_z \underline{z}). \end{aligned} \quad (7b)$$

By substituting Eqs. (2a), (2b), (6a), and (6b) into Eqs. (7a) and (7b), we can obtain the following coupled linear algebra equations of Fourier coefficients,

$$jk_{z,q}E_{y,h,q} = k_0 \sum_g \sum_p \tilde{\mu}_{h-g,q-p} H_{x,g,p} + jk_y E_{z,h,q}, \quad (8a)$$

$$jk_{z,q}E_{x,h,q} = -k_0 \sum_g \sum_p \tilde{\mu}_{h-g,q-p} H_{y,h,p} + jk_{x,h} E_{z,h,q}, \quad (8b)$$

$$\sum_g \sum_p \tilde{\epsilon}_{h-g,q-p} E_{z,g,p} = -\frac{jk_{x,h}}{k_0} H_{y,h,q} + \frac{jk_y}{k_0} H_{x,h,q}, \quad (8c)$$

$$\frac{jk_{z,q}}{k_0} H_{y,h,q} = \sum_g \sum_p \tilde{\epsilon}_{h-g,q-p} E_{x,g,p} + \frac{jk_y}{k_0} H_{z,h,q}, \quad (8d)$$

$$\frac{jk_{z,q}}{k_0} H_{x,h,q} = -\sum_g \sum_p \tilde{\epsilon}_{h-g,q-p} E_{y,g,p} + \frac{jk_{x,h}}{k_0} H_{z,h,q}, \quad (8e)$$

$$\sum_g \sum_p \tilde{\mu}_{h-g,q-p} H_{z,g,p} = \frac{-jk_{x,h}}{k_0} E_{y,h,q} + \frac{jk_y}{k_0} E_{x,h,q}, \quad (8f)$$

where  $k_{z,q}$  is defined by

$$k_{z,q} = k_{z,0} + G_{z,q}. \quad (8g)$$

We can arrange Eqs. (8a)–(8f) into an algebraic matrix eigenvalue equation. Let  $\underline{\epsilon}$ ,  $\underline{\mu}$ ,  $\underline{\alpha}$ , and  $\underline{\beta}$  be the Toeplitz matrices of the permittivity, permeability, reciprocal permittivity, and reciprocal permeability functions, respectively. The Toeplitz matrix of the permittivity  $\underline{\epsilon}$  is given by

$$\underline{\epsilon} = \begin{pmatrix} \underline{\epsilon}_0 & \underline{\epsilon}_{-1} & \cdots & \underline{\epsilon}_{-2H} \\ \underline{\epsilon}_1 & \underline{\epsilon}_0 & & \underline{\epsilon}_{-2H+1} \\ \vdots & \vdots & & \\ \underline{\epsilon}_{2H} & \underline{\epsilon}_{2H-1} & \cdots & \underline{\epsilon}_0 \end{pmatrix}, \quad (9a)$$

where  $\underline{\epsilon}_k$  is given by

$$\underline{\epsilon}_k = \begin{pmatrix} \tilde{\epsilon}_{k,0} & \tilde{\epsilon}_{k,-1} & \cdots & \tilde{\epsilon}_{k,-2Q} \\ \tilde{\epsilon}_{k,1} & \tilde{\epsilon}_{k,0} & & \tilde{\epsilon}_{k,-2Q+1} \\ \vdots & \vdots & & \\ \tilde{\epsilon}_{k,2Q} & \tilde{\epsilon}_{k,2Q-1} & \cdots & \tilde{\epsilon}_{k,0} \end{pmatrix}. \quad (9b)$$

The Toeplitz matrices of permeability  $\underline{\mu}$ , reciprocal permittivity  $\underline{\alpha}$ , and reciprocal permeability  $\underline{\beta}$  are defined similarly to that of permittivity. In addition,  $\underline{K}_x$ ,  $\underline{K}_y$ , and  $\underline{K}_z$  are defined by, respectively,

$$\underline{K}_x = \begin{pmatrix} \frac{k_{x,-H}}{k_0} \underline{I}_{(2Q+1)} & 0 & \cdots & 0 \\ 0 & \frac{k_{x,-H+1}}{k_0} \underline{I}_{(2Q+1)} & 0 & 0 \\ \vdots & \vdots & \ddots & 0 \\ 0 & 0 & \cdots & \frac{k_{x,H}}{k_0} \underline{I}_{(2Q+1)} \end{pmatrix}, \quad (10a)$$

$$\underline{K}_y = \left( \frac{k_y}{k_0} \right) \underline{I}_{(2Q+1)(2H+1)}, \quad (10b)$$

$$\underline{K}_z = \begin{pmatrix} \left[ \frac{k_{z,q}}{k_0} \right] & 0 & \cdots & 0 \\ 0 & \left[ \frac{k_{z,q}}{k_0} \right] & 0 & 0 \\ \vdots & \vdots & \left[ \frac{k_{z,q}}{k_0} \right] & 0 \\ 0 & 0 & \cdots & \left[ \frac{k_{z,q}}{k_0} \right] \end{pmatrix}, \quad (10c)$$

where  $\underline{I}_N$  is the  $N \times N$  identity matrix and  $[k_{z,q}/k_0]$  is defined by

$$\begin{bmatrix} k_{z,q} \\ k_0 \end{bmatrix} = \begin{pmatrix} \frac{k_{z,-Q}}{k_0} & 0 & \cdots & 0 \\ 0 & \frac{k_{z,-(Q-1)}}{k_0} & 0 & 0 \\ \vdots & \vdots & \ddots & 0 \\ 0 & 0 & \cdots & \frac{k_{z,Q}}{k_0} \end{pmatrix}. \quad (10d)$$

$$\begin{bmatrix} G_{z,q} \\ k_0 \end{bmatrix} = \begin{pmatrix} \frac{G_{z,-Q}}{k_0} & 0 & \cdots & 0 \\ 0 & \frac{G_{z,-(Q-1)}}{k_0} & 0 & 0 \\ \vdots & \vdots & \ddots & 0 \\ 0 & 0 & \cdots & \frac{G_{z,Q}}{k_0} \end{pmatrix}. \quad (10g)$$

From Eq. (8g), we can see that

$$\underline{\underline{K}}_z = \frac{k_{z,0}}{k_0} \underline{\underline{I}}_{(2Q+1)(2H+1)} + \underline{\underline{G}}_z, \quad (10e)$$

where  $\underline{\underline{G}}_x$  is defined by

$$\underline{\underline{G}}_z = \begin{pmatrix} \begin{bmatrix} \frac{G_{z,q}}{k_0} \\ \frac{G_{z,q}}{k_0} \end{bmatrix} & 0 & \cdots & 0 \\ 0 & \begin{bmatrix} \frac{G_{z,q}}{k_0} \\ \frac{G_{z,q}}{k_0} \end{bmatrix} & 0 & 0 \\ \vdots & \vdots & \begin{bmatrix} \frac{G_{z,q}}{k_0} \\ \frac{G_{z,q}}{k_0} \end{bmatrix} & 0 \\ 0 & 0 & \cdots & \begin{bmatrix} \frac{G_{z,q}}{k_0} \\ \frac{G_{z,q}}{k_0} \end{bmatrix} \end{pmatrix}, \quad (10f)$$

where  $[G_{z,q}/k_0]$  is defined by

Let the vector notation  $\underline{E}_x$  be defined by

$$\begin{aligned} \underline{E}_x = & [[E_{x,-H,-Q} \cdots E_{x,-H,Q}] \\ & \times [E_{x,-H+1,-Q} \cdots E_{x,-H+1,Q}] \cdots [E_{x,H,-Q} \cdots E_{x,H,Q}]]^t. \end{aligned} \quad (11)$$

$\underline{E}_y$ ,  $\underline{E}_z$ ,  $\underline{H}_x$ ,  $\underline{H}_y$ , and  $\underline{H}_z$  are equivalently defined. With use of the above notation, the algebraic equation system of Eqs. (8a)–(8f) is reformulated to

$$\begin{bmatrix} \underline{\underline{\varepsilon}} & 0 & 0 & 0 & 0 & 0 \\ 0 & \underline{\underline{\varepsilon}} & 0 & 0 & 0 & 0 \\ 0 & 0 & \underline{\underline{\varepsilon}} & 0 & 0 & 0 \\ 0 & 0 & 0 & \underline{\underline{\mu}} & 0 & 0 \\ 0 & 0 & 0 & 0 & \underline{\underline{\mu}} & 0 \\ 0 & 0 & 0 & 0 & 0 & \underline{\underline{\mu}} \end{bmatrix} \begin{bmatrix} \underline{E}_x \\ \underline{E}_y \\ \underline{E}_z \\ \underline{H}_x \\ \underline{H}_y \\ \underline{H}_z \end{bmatrix} = \begin{bmatrix} 0 & 0 & 0 & 0 & j\underline{\underline{K}}_z & -j\underline{\underline{K}}_y \\ 0 & 0 & 0 & -j\underline{\underline{K}}_z & 0 & j\underline{\underline{K}}_x \\ 0 & 0 & 0 & j\underline{\underline{K}}_y & -j\underline{\underline{K}}_x & 0 \\ 0 & j\underline{\underline{K}}_z & -j\underline{\underline{K}}_y & 0 & 0 & 0 \\ -j\underline{\underline{K}}_z & 0 & j\underline{\underline{K}}_x & 0 & 0 & 0 \\ j\underline{\underline{K}}_y & -j\underline{\underline{K}}_x & 0 & 0 & 0 & 0 \end{bmatrix} \begin{bmatrix} \underline{E}_x \\ \underline{E}_y \\ \underline{E}_z \\ \underline{H}_x \\ \underline{H}_y \\ \underline{H}_z \end{bmatrix}. \quad (12a)$$

We can simply extend the above isotropic equation to the more general anisotropic version as

$$\begin{bmatrix} \underline{\underline{\varepsilon}}^{(x)} & 0 & 0 & 0 & 0 & 0 \\ 0 & \underline{\underline{\varepsilon}}^{(y)} & 0 & 0 & 0 & 0 \\ 0 & 0 & \underline{\underline{\varepsilon}}^{(z)} & 0 & 0 & 0 \\ 0 & 0 & 0 & \underline{\underline{\mu}}^{(x)} & 0 & 0 \\ 0 & 0 & 0 & 0 & \underline{\underline{\mu}}^{(y)} & 0 \\ 0 & 0 & 0 & 0 & 0 & \underline{\underline{\mu}}^{(z)} \end{bmatrix} \begin{bmatrix} \underline{E}_x \\ \underline{E}_y \\ \underline{E}_z \\ \underline{H}_x \\ \underline{H}_y \\ \underline{H}_z \end{bmatrix} = \begin{bmatrix} 0 & 0 & 0 & 0 & j\underline{\underline{K}}_z & -j\underline{\underline{K}}_y \\ 0 & 0 & 0 & -j\underline{\underline{K}}_z & 0 & j\underline{\underline{K}}_x \\ 0 & 0 & 0 & j\underline{\underline{K}}_y & -j\underline{\underline{K}}_x & 0 \\ 0 & j\underline{\underline{K}}_z & -j\underline{\underline{K}}_y & 0 & 0 & 0 \\ -j\underline{\underline{K}}_z & 0 & j\underline{\underline{K}}_x & 0 & 0 & 0 \\ j\underline{\underline{K}}_y & -j\underline{\underline{K}}_x & 0 & 0 & 0 & 0 \end{bmatrix} \begin{bmatrix} \underline{E}_x \\ \underline{E}_y \\ \underline{E}_z \\ \underline{H}_x \\ \underline{H}_y \\ \underline{H}_z \end{bmatrix}. \quad (12b)$$

Since the transverse wavevector components  $k_{x,h}$  and  $k_y$  are predetermined, Eq. (12b) is rearranged as an eigenvalue matrix equation with respect to the  $z$ -direction wavevector component,  $k_{z,0}$ , which is called the propagation constant. By eliminating  $\underline{E}_z$  and  $\underline{H}_z$  using the relations

$$\underline{E}_z = \underline{\varepsilon}_{(z)}^{-1}(-j\underline{K}_x \underline{H}_y + j\underline{K}_y \underline{H}_x), \quad (13a)$$

$$\underline{H}_z = \underline{\mu}_{(z)}^{-1}(-j\underline{K}_x \underline{E}_y + j\underline{K}_y \underline{E}_x), \quad (13b)$$

and Eq. (10e), Eq. (12b) is manipulated into the form

$$\begin{bmatrix} 0 & 0 & \underline{K}_y \underline{\varepsilon}_{(z)}^{-1} \underline{K}_x & \underline{\mu}_{(x)} - \underline{K}_y \underline{\varepsilon}_{(z)}^{-1} \underline{K}_y \\ 0 & 0 & -\underline{\mu}_{(y)} + \underline{K}_x \underline{\varepsilon}_{(z)}^{-1} \underline{K}_x & -\underline{K}_x \underline{\varepsilon}_{(z)}^{-1} \underline{K}_y \\ \underline{K}_y \underline{\mu}_{(z)}^{-1} \underline{K}_x & \underline{\varepsilon}_{(x)} - \underline{K}_y \underline{\mu}_{(z)}^{-1} \underline{K}_y & 0 & 0 \\ -\underline{\varepsilon}_{(y)} + \underline{K}_x \underline{\mu}_{(z)}^{-1} \underline{K}_x & -\underline{K}_x \underline{\mu}_{(z)}^{-1} \underline{K}_y & 0 & 0 \end{bmatrix} \begin{bmatrix} \underline{E}_y \\ \underline{E}_x \\ \underline{H}_y \\ \underline{H}_x \end{bmatrix} = j \frac{k_{z,0}}{k_0} \begin{bmatrix} \underline{E}_y \\ \underline{E}_x \\ \underline{H}_y \\ \underline{H}_x \end{bmatrix} + \begin{bmatrix} j\underline{G}_z & 0 & 0 & 0 \\ 0 & j\underline{G}_z & 0 & 0 \\ 0 & 0 & j\underline{G}_z & 0 \\ 0 & 0 & 0 & j\underline{G}_z \end{bmatrix} \begin{bmatrix} \underline{E}_y \\ \underline{E}_x \\ \underline{H}_y \\ \underline{H}_x \end{bmatrix}. \quad (14a)$$

Then we can obtain a matrix eigenvalue equation with respect to  $k_{z,0}$  as

$$\begin{bmatrix} -j\underline{G}_z & 0 & \underline{K}_y \underline{\varepsilon}_{(z)}^{-1} \underline{K}_x & \underline{\mu}_{(x)} - \underline{K}_y \underline{\varepsilon}_{(z)}^{-1} \underline{K}_y \\ 0 & -j\underline{G}_z & -\underline{\mu}_{(y)} + \underline{K}_x \underline{\varepsilon}_{(z)}^{-1} \underline{K}_x & -\underline{K}_x \underline{\varepsilon}_{(z)}^{-1} \underline{K}_y \\ \underline{K}_y \underline{\mu}_{(z)}^{-1} \underline{K}_x & \underline{\varepsilon}_{(x)} - \underline{K}_y \underline{\mu}_{(z)}^{-1} \underline{K}_y & -j\underline{G}_z & 0 \\ -\underline{\varepsilon}_{(y)} + \underline{K}_x \underline{\mu}_{(z)}^{-1} \underline{K}_x & -\underline{K}_x \underline{\mu}_{(z)}^{-1} \underline{K}_y & 0 & -j\underline{G}_z \end{bmatrix} \begin{bmatrix} \underline{E}_y \\ \underline{E}_x \\ \underline{H}_y \\ \underline{H}_x \end{bmatrix} = \frac{jk_{z,0}}{k_0} \begin{bmatrix} \underline{E}_y \\ \underline{E}_x \\ \underline{H}_y \\ \underline{H}_x \end{bmatrix}. \quad (14b)$$

It is noted that in a practical implementation of Eq. (14b), the Fourier factorization rule [3–7] for the  $x$ - and  $z$ -direction polarization should be properly considered for achieving good convergence. However, in this paper, for convenience, a simple empirical method for 2-D gratings proposed by Lalanne [2] is employed for practical simulations. Following Lalanne's approach, we set  $\underline{\varepsilon}_{(x)}$ ,  $\underline{\varepsilon}_{(y)}$ ,  $\underline{\varepsilon}_{(z)}$ ,  $\underline{\mu}_{(x)}$ ,  $\underline{\mu}_{(y)}$ , and  $\underline{\mu}_{(z)}$  as

$$\underline{\varepsilon}_{(x)} = t_x \underline{\varepsilon} + (1 - t_x) \underline{\alpha}^{-1}, \quad (15a)$$

$$\underline{\varepsilon}_{(y)} = t_y \underline{\varepsilon} + (1 - t_y) \underline{\alpha}^{-1}, \quad (15b)$$

$$\underline{\varepsilon}_{(z)} = t_z \underline{\varepsilon} + (1 - t_z) \underline{\alpha}^{-1}, \quad (15c)$$

$$\underline{\mu}_{(x)} = s_x \underline{\mu} + (1 - s_x) \underline{\beta}^{-1}, \quad (15d)$$

$$\underline{\mu}_{(y)} = s_y \underline{\mu} + (1 - s_y) \underline{\beta}^{-1}, \quad (15e)$$

$$\underline{\mu}_{(z)} = s_z \underline{\mu} + (1 - s_z) \underline{\beta}^{-1}. \quad (15f)$$

By default, the permeability components are taken as constant. In the analysis of one-dimensionally periodic (along the  $x$ -direction) binary gratings placed on the  $x$ - $y$  plane, according to the Fourier factorization rule,  $\underline{\varepsilon}_{(x)}$ ,  $\underline{\varepsilon}_{(y)}$ , and  $\underline{\varepsilon}_{(z)}$ —with  $t_x$ ,  $t_z$ , and  $t_y$  being set to 0, 1, and 1, respectively—are given by  $\underline{\varepsilon}_{(x)} = \underline{\alpha}^{-1}$ ,  $\underline{\varepsilon}_{(y)} = \underline{\varepsilon}$ , and  $\underline{\varepsilon}_{(z)} = \underline{\varepsilon}$ , respectively. For the 1-D periodic metallic triangle grating with 45-deg base angle analyzed in Section 4,  $t_x$ ,  $t_z$ , and  $t_y$  are set to 0.5, 0.5, and 1, respectively.

It is noted that a degeneracy problem [12,13] exists in Eq. (14b). Since the dimensions of the system matrix are  $4(2H+1)(2Q+1) \times 4(2H+1)(2Q+1)$ , the total number of obtained eigensolutions is  $4(2H+1)(2Q+1)$ . As discussed in [13], the eigenvalues  $k_{z,0}$  must be extracted in the first Brillouin zone using the eigenvalue selection rule

$$-G_z/2 \leq \text{Re}(k_{z,0}) < G_z/2. \quad (16)$$

We can choose  $4(2H+1)$  eigenmodes in the first Brillouin zone among the obtained  $4(2H+1)(2Q+1)$  eigenmodes. From the mathematical point of view, the asymmetrically truncated pseudo-Fourier series of electromagnetic fields can also be solutions of the eigenvalue equation (14b). The eigenvalues in the other Brillouin zones are physically degenerate with corresponding eigenvalues in the first Brillouin zone. However, since the asymmetrically truncated pseudo-Fourier series shows poor convergence, the symmetrically truncated pseudo-Fourier series, that is, the solution in the first Brillouin zone, is taken as the default expression of the Bloch eigenmodes. The system matrix size of  $4(2H+1)(2Q+1) \times 4(2H+1)(2Q+1)$  renders full-frequency formalism such as PFMA impracticable by increasing computing cost dramatically. This difficult degeneracy problem, inherent in the described full-frequency PFMA, remains to be overcome. Nevertheless, the study of full-frequency schemes such as PFMA is meaningful in that it can provide in-depth understanding of the Fourier analysis of the linear Maxwell equations.

After obtaining the eigenvalues and eigenvectors of the main eigenvalue equation, we must classify the obtained

eigenmodes into two categories, positive (forward) modes and negative (backward) modes, with respect to eigenvalues possessing one of the forms  $jk_{z,0}^{(g)}=a^{(g)}+jb^{(g)}$ ,  $jk_{z,0}^{(g)}=a^{(g)}-jb^{(g)}$ ,  $jk_{z,0}^{(g)}=-a^{(g)}+jb^{(g)}$ , or  $jk_{z,0}^{(g)}=-a^{(g)}-jb^{(g)}$ , where  $a^{(g)}>0$  and  $b^{(g)}>0$ . The eigenmodes with eigenvalues of  $jk_{z,0}^{(g)}=a^{(g)}+jb^{(g)}$  or  $jk_{z,0}^{(g)}=-a^{(g)}-jb^{(g)}$  are referred to as negative modes, and the notation  $k_{z,0}^{(g)-}$  with the minus superscript is used to indicate the negative modes. The eigenmodes with eigenvalues of  $jk_{z,0}^{(g)}=-a^{(g)}+jb^{(g)}$  and  $jk_{z,0}^{(g)}=a^{(g)}-jb^{(g)}$  are referred to as positive modes, and the notation  $k_{z,0}^{(g)+}$  with the plus superscript is used to indicate the positive mode. In particular, the eigenmodes that have pure real eigenvalues of  $jk_{z,0}^{(g)}=jb^{(g)}$  and  $jk_{z,0}^{(g)}=-jb^{(g)}$  with  $a^{(g)}=0$  are classified as the positive modes. With these terms, the  $g$ th positive eigenmode ( $\underline{E}_{(g)}^+$ ,  $\underline{H}_{(g)}^+$ ) and the  $g$ th negative eigenmode ( $\underline{E}_{(g)}^-$ ,  $\underline{H}_{(g)}^-$ ) are represented, respectively, by

$$\underline{E}_{(g)}^+(x,y,z) = \sum_{h=-H}^H \sum_{q=-Q}^Q (E_{x,h,q}^{(g)+} \hat{x} + E_{y,h,q}^{(g)+} \hat{y} + E_{z,h,q}^{(g)+} \hat{z}) \times \exp[j(k_{x,h}x + k_{y,q}y + k_{z,q}^{(g)+}z)], \quad (17a)$$

$$\underline{E}_{(g)}^-(x,y,z) = \sum_{h=-H}^H \sum_{q=-Q}^Q (E_{x,h,q}^{(g)-} \hat{x} + E_{y,h,q}^{(g)-} \hat{y} + E_{z,h,q}^{(g)-} \hat{z}) \times \exp\{j[k_{x,h}x + k_{y,q}y + k_{z,q}^{(g)-}(z - \Delta d)]\}, \quad (17b)$$

$$\underline{H}_{(g)}^+(x,y,z) = j \sqrt{\frac{\epsilon_0}{\mu_0}} \sum_{h=-H}^H \sum_{q=-Q}^Q (H_{x,h,q}^{(g)+} \hat{x} + H_{y,h,q}^{(g)+} \hat{y} + H_{z,h,q}^{(g)+} \hat{z}) \times \exp[j(k_{x,h}x + k_{y,q}y + k_{z,q}^{(g)+}z)], \quad (17c)$$

$$\underline{H}_{(g)}^-(x,y,z) = j \sqrt{\frac{\epsilon_0}{\mu_0}} \sum_{h=-H}^H \sum_{q=-Q}^Q (H_{x,h,q}^{(g)-} \hat{x} + H_{y,h,q}^{(g)-} \hat{y} + H_{z,h,q}^{(g)-} \hat{z}) \times \exp\{j[k_{x,h}x + k_{y,q}y + k_{z,q}^{(g)-}(z - \Delta d)]\}. \quad (17d)$$

Here, for convenience, the mode index is denoted by  $g$  instead of  $k$ . Also, it is noted that the exponential term of the negative mode ( $\underline{E}_{(g)}^-$ ,  $\underline{H}_{(g)}^-$ ) is given by  $\exp\{j[k_{x,h}x + k_{y,q}y + k_{z,q}^{(g)-}(z - \Delta d)]\}$ , which is the point modified from Eqs. (6a) and (6b). The number of positive modes and that of negative modes are denoted by  $M^+$  and  $M^-$ , respectively. The sum of  $M^+$  and  $M^-$  is  $M^+ + M^- = 4(2H + 1)$ .

The total electromagnetic fields in the grating region can be represented by the superposition of the obtained eigenmodes as follows:

$$\underline{E}(x,y,z) = \sum_{g=1}^{M^+} C_g^+ \underline{E}_{(g)}^+(x,y,z) + \sum_{g=1}^{M^-} C_g^- \underline{E}_{(g)}^-(x,y,z), \quad (18a)$$

$$\underline{H}(x,y,z) = \sum_{g=1}^{M^+} C_g^+ \underline{H}_{(g)}^+(x,y,z) + \sum_{g=1}^{M^-} C_g^- \underline{H}_{(g)}^-(x,y,z), \quad (18b)$$

where  $C_g^+$  and  $C_g^-$  are the coupling coefficients of the positive mode and the negative mode, respectively. As manifested in [13], the boundary conditions at both boundaries  $z=0$  and  $z=\Delta d$  are given, respectively, by

$$\begin{bmatrix} I & 0 & I & 0 \\ 0 & I & 0 & I \\ \frac{k_{x,h}k_y}{k_0k_{I,z,h}} & \frac{(k_{I,z,h}^2 + k_{x,h}^2)}{k_0k_{I,z,h}} & \frac{k_{x,h}k_y}{k_0k_{I,z,h}} & \frac{(k_{I,z,h}^2 + k_{x,h}^2)}{k_0k_{I,z,h}} \\ \frac{(k_y^2 + k_{I,z,h}^2)}{k_0k_{I,z,h}} & \frac{k_yk_{x,h}}{k_0k_{I,z,h}} & \frac{(k_y^2 + k_{I,z,h}^2)}{k_0k_{I,z,h}} & \frac{k_yk_{x,h}}{k_0k_{I,z,h}} \end{bmatrix} \begin{bmatrix} u_y \delta_{hs} \\ u_x \delta_{hs} \\ R_{y,h} \\ R_{x,h} \end{bmatrix} = \begin{pmatrix} \sum_{q=-Q}^Q E_{y,h,q}^{(1)+} & \cdots & \sum_{q=-Q}^Q E_{y,h,q}^{(M^+)+} & \sum_{q=-Q}^Q E_{y,h,q}^{(1)-} e^{-j(qG_z + k_z^{(1)-})\Delta d} & \cdots & \sum_{q=-Q}^Q E_{y,h,q}^{(M^-)-} e^{-j(qG_z + k_z^{(M^-)-})\Delta d} \\ \sum_{q=-Q}^Q E_{x,h,q}^{(1)+} & \cdots & \sum_{q=-Q}^Q E_{x,h,q}^{(M^+)+} & \sum_{q=-Q}^Q E_{x,h,q}^{(1)-} e^{-j(qG_z + k_z^{(1)-})\Delta d} & \cdots & \sum_{p=-Q}^Q E_{x,h,q}^{(M^-)-} e^{-j(qG_z + k_z^{(M^-)-})\Delta d} \\ j \sum_{q=-Q}^Q H_{y,h,q}^{(1)+} & \cdots & j \sum_{q=-Q}^Q H_{y,h,q}^{(M^+)+} & j \sum_{q=-Q}^Q H_{y,h,q}^{(1)-} e^{-j(qG_z + k_z^{(1)-})\Delta d} & \cdots & j \sum_{p=-Q}^Q H_{y,h,q}^{(M^-)-} e^{-j(qG_z + k_z^{(M^-)-})\Delta d} \\ j \sum_{p=-Q}^Q H_{x,h,q}^{(1)+} & \cdots & j \sum_{q=-Q}^Q H_{x,h,q}^{(M^+)+} & j \sum_{q=-Q}^Q H_{x,h,q}^{(1)-} e^{-j(qG_z + k_z^{(1)-})\Delta d} & \cdots & j \sum_{p=-Q}^Q H_{x,h,q}^{(M^-)-} e^{-j(qG_z + k_z^{(M^-)-})\Delta d} \end{pmatrix} \begin{bmatrix} C_1^+ \\ \vdots \\ C_{M^+}^+ \\ C_1^- \\ \vdots \\ C_{M^-}^- \end{bmatrix}, \quad (19a)$$

$$= \begin{pmatrix} \sum_{q=-Q}^Q E_{y,h,q}^{(1)+} e^{j(qG_z+k_z^{(1)+})\Delta d} & \dots & \sum_{q=-Q}^Q E_{y,h,q}^{(M^+)+} e^{j(qG_z+k_z^{(M^+)+})\Delta d} & \sum_{q=-Q}^Q E_{y,h,q}^{(1)-} & \dots & \sum_{q=-Q}^Q E_{y,h,q}^{(M^-)-} \\ \sum_{q=-Q}^Q E_{x,h,q}^{(1)+} e^{j(qG_z+k_z^{(1)+})\Delta d} & \dots & \sum_{q=-Q}^Q E_{x,h,q}^{(M^+)+} e^{j(qG_z+k_z^{(M^+)+})\Delta d} & \sum_{q=-Q}^Q E_{x,h,q}^{(1)-} & \dots & \sum_{p=-Q}^Q E_{x,h,q}^{(M^-)-} \\ j \sum_{q=-Q}^Q H_{y,h,q}^{(1)+} e^{j(qG_z+k_z^{(1)+})\Delta d} & \dots & j \sum_{q=-Q}^Q H_{y,h,q}^{(M^+)+} e^{j(qG_z+k_z^{(M^+)+})\Delta d} & j \sum_{q=-Q}^Q H_{y,h,q}^{(1)-} & \dots & j \sum_{p=-Q}^Q H_{y,h,q}^{(M^-)-} \\ j \sum_{p=-Q}^Q H_{x,h,q}^{(1)+} e^{j(qG_z+k_z^{(1)+})\Delta d} & \dots & j \sum_{q=-Q}^Q H_{x,h,q}^{(M^+)+} e^{j(qG_z+k_z^{(M^+)+})\Delta d} & j \sum_{q=-Q}^Q H_{x,h,q}^{(1)-} & \dots & j \sum_{p=-Q}^Q H_{x,h,q}^{(M^-)-} \end{pmatrix} \begin{bmatrix} T_{y,h} \\ T_{x,h} \\ C_1^+ \\ \vdots \\ C_{M^+}^+ \\ C_1^- \\ \vdots \\ C_{M^-}^- \end{bmatrix}. \quad (19b)$$

By solving Eqs. (19a) and (19b), we can obtain the reflection and transmission coefficients ( $R_{x,h}, R_{y,h}, R_{z,h}$ ) and ( $T_{x,h}, T_{y,h}, T_{z,h}$ ), and the coupling coefficients ( $C_1^+, \dots, C_{M^+}^+, C_1^-, \dots, C_{M^-}^-$ ).

The extension of the PFMA to 3-D theory can be straightforwardly achieved since the process of mathematical extension to the 3-D PFMA is precisely the same as that for the 2-D PFMA. In next section, the described PFMA on a single layer is extended to multilayer structure analysis with use of the ESMM.

### 3. MULTILAYER STRUCTURE ANALYSIS WITH THE EXTENDED SCATTERING MATRIX METHOD

Basically, in the full-dimension (2-D) Fourier representation scheme used in the PFMA, the longitudinal-direction ( $z$ -direction) Fourier spectral components in a wide enough spectral bandwidth must be retained for accurately modeling the discontinuous profiles involved in the target structures. When the  $z$ -direction Fourier spectral bandwidth to be retained is fixed, we can see that as the  $z$ -direction period  $\Delta d$  becomes longer, the required number of  $z$ -direction Fourier spectral components must increase to cover the required full-Fourier spectral bandwidth. Hence, in a practical computation, the  $z$ -direction period  $\Delta d$  is inevitably limited in a certain specific range that is dependent on the structural parameters of the target structure to be analyzed, since the number of  $z$ -directional Fourier spectral components that are manageable with practical computers is restricted. Therefore, to practically analyze longer or deeper structures, we should take the multilayer modeling scheme with the SMM [9,10].

In this section, the general analysis scheme based on the PFMA and the ESMM for multilayer structures is de-

scribed. First, each single layer in a multilayer structure is characterized by the PFMA, and the characterization results of each single layer are combined by the ESMM to find the total characteristics of the multilayer. In [10], the ESMM is applied to the RCWA. However, without significant modifications, we can also straightforwardly apply the ESMM to the PFMA to analyze multilayer structures. See [10] for complete details about the ESMM.

Let us consider the multilayer modeling of the grating structure shown in Fig. 1. The  $n$ th layer is bidirectional characterized with the PFMA as indicated in Figs. 4(a) and 4(b). For the left-to-right characterization indicated in Fig. 4(a), the boundary-condition matching equations (19a) and (19b) are expressed as the following matrix operator equations,

$$\begin{pmatrix} \mathbf{W}_h & \mathbf{W}_h \\ \mathbf{V}_h & -\mathbf{V}_h \end{pmatrix} \begin{pmatrix} \vec{\mathbf{U}}^{(n,n)} \\ \vec{\mathbf{R}}^{(n,n)} \end{pmatrix} = \begin{pmatrix} \mathbf{W}_+^{(n)} & \mathbf{W}_-^{(n)} \mathbf{X}_-^{(n)} \\ \mathbf{V}_+^{(n)} & \mathbf{V}_-^{(n)} \mathbf{X}_-^{(n)} \end{pmatrix} \begin{pmatrix} \mathbf{C}_a^{(n,n)+} \\ \mathbf{C}_a^{(n,n)-} \end{pmatrix}, \quad (20a)$$

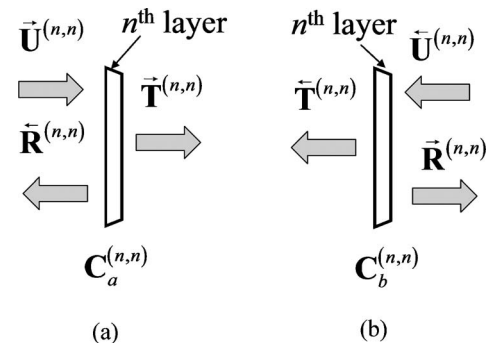


Fig. 4. Bidirectional characterization of the  $n$ th layer: (a) left-to-right characterization, (b) right-to-left characterization.

$$\begin{pmatrix} \mathbf{W}_+^{(n)} \mathbf{X}_+^{(n)} & \mathbf{W}_-^{(n)} \\ \mathbf{V}_+^{(n)} \mathbf{X}_+^{(n)} & \mathbf{V}_-^{(n)} \end{pmatrix} \begin{pmatrix} \mathbf{C}_a^{(n,n)+} \\ \mathbf{C}_a^{(n,n)-} \end{pmatrix} = \begin{pmatrix} \mathbf{W}_h & \mathbf{W}_h \\ \mathbf{V}_h & -\mathbf{V}_h \end{pmatrix} \begin{pmatrix} \tilde{\mathbf{T}}^{(n,n)} \\ \mathbf{0} \end{pmatrix}, \quad (20b)$$

where  $\mathbf{W}_h$  and  $\mathbf{V}_h$  are  $[2(2H+1)] \times [2(2H+1)]$  matrices and are given, respectively, by

$$\mathbf{W}_h = \begin{pmatrix} \mathbf{I} & \mathbf{0} \\ \mathbf{0} & \mathbf{I} \end{pmatrix}, \quad (20c)$$

$$\mathbf{V}_h = \begin{pmatrix} \begin{bmatrix} k_{x,h} k_y \\ k_0 k_{I,z,h} \end{bmatrix} & \begin{bmatrix} (k_{I,z,h}^2 + k_{x,h}^2) \\ k_0 k_{I,z,h} \end{bmatrix} \\ \begin{bmatrix} (k_y^2 + k_{I,z,h}^2) \\ -k_0 k_{I,z,h} \end{bmatrix} & \begin{bmatrix} -k_y k_{x,h} \\ -k_0 k_{I,z,h} \end{bmatrix} \end{pmatrix}, \quad (20d)$$

where  $\mathbf{I}$  and  $\mathbf{0}$  are the  $(2H+1) \times (2H+1)$  identity matrix and the zero matrix, respectively, and  $[a_h]$  means a  $(2H+1) \times (2H+1)$  diagonal matrix given by the

$$\begin{pmatrix} a_{-H} & \cdots & 0 \\ \vdots & \ddots & \vdots \\ 0 & \cdots & a_H \end{pmatrix}. \quad (20e)$$

$\mathbf{W}_+^{(n)}$  and  $\mathbf{V}_+^{(n)}$  are  $[2(2H+1)] \times M^+$  matrices indicating the part of the positive modes in Eq. (19a).  $\mathbf{W}_-^{(n)}$  and  $\mathbf{V}_-^{(n)}$  are

$$\begin{pmatrix} \mathbf{C}_a^{(n,n)+} \\ \mathbf{C}_a^{(n,n)-} \end{pmatrix} = \begin{pmatrix} \mathbf{W}_h^{-1} \mathbf{W}_+^{(n)} + \mathbf{V}_h^{-1} \mathbf{V}_+^{(n)} \\ (\mathbf{W}_h^{-1} \mathbf{W}_+^{(n)} - \mathbf{V}_h^{-1} \mathbf{V}_+^{(n)}) \mathbf{X}_+^{(n)} \end{pmatrix}^{-1} \begin{pmatrix} 2\tilde{\mathbf{U}}^{(n,n)} \\ \mathbf{0} \end{pmatrix}, \quad (21a)$$

$$\tilde{\mathbf{R}}^{(n,n)} = \mathbf{W}_h^{-1} [\mathbf{W}_+^{(n)} \mathbf{C}_a^{(n,n)+} + \mathbf{W}_-^{(n)} \mathbf{X}_-^{(n)} \mathbf{C}_a^{(n,n)-} - \mathbf{W}_h \tilde{\mathbf{U}}^{(n,n)}], \quad (21b)$$

$$\tilde{\mathbf{T}}^{(n,n)} = \mathbf{W}_h^{-1} [\mathbf{W}_+^{(n)} \mathbf{X}_+^{(n)} \mathbf{C}_a^{(n,n)+} + \mathbf{W}_-^{(n)} \mathbf{C}_a^{(n,n)-}]. \quad (21c)$$

The  $[4(2H+1)] \times [2(2H+1)]$  coupling coefficient matrix operator  $\mathbf{C}_a^{(n,n)}$  is defined by

$$\mathbf{C}_a^{(n,n)} = (\mathbf{C}_a^{(n,n)+} \quad \mathbf{C}_a^{(n,n)-})^t. \quad (21d)$$

In the same way, the coupling coefficient matrix operators  $\mathbf{C}_b^{(n,n)} = (\mathbf{C}_b^{(n,n)+} \quad \mathbf{C}_b^{(n,n)-})^t$  and the reflection and transmission operators  $\tilde{\mathbf{R}}^{(n,n)}$  and  $\tilde{\mathbf{T}}^{(n,n)}$  of the right-to-left characterization can be obtained.

Conventionally, the  $S$  matrix of the single layer,  $\mathbf{S}^{(n,n)}$ , is defined by

$$\mathbf{S}^{(n,n)} = \begin{pmatrix} \tilde{\mathbf{T}}^{(n,n)} & \tilde{\mathbf{R}}^{(n,n)} \\ \tilde{\mathbf{R}}^{(n,n)} & \tilde{\mathbf{T}}^{(n,n)} \end{pmatrix}. \quad (22)$$

The directional characteristics of any multilayer can be obtained by properly combining the obtained matrix operators of single layers through Redheffer's star product relation.

Figure 5 shows the bidirectional characterization of a multilayer composed of two neighboring layers, the  $n$ th

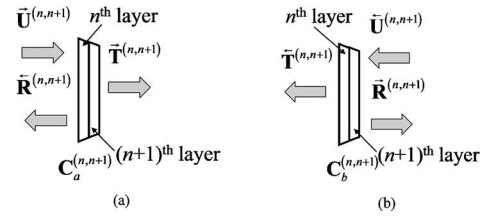


Fig. 5. Bidirectional characterization of a multilayer composed of two neighboring layers: (a) left-to-right characterization, (b) right-to-left characterization.

$[2(2H+1)] \times M^-$  matrices indicating the part of the negative modes in Eq. (19b).  $\tilde{\mathbf{U}}^{(n,n)}$  is the input operator—actually, a  $[2(2H+1)] \times [2(2H+1)]$  identity matrix.  $\tilde{\mathbf{R}}^{(n,n)}$  and  $\tilde{\mathbf{T}}^{(n,n)}$  are referred to as the reflection coefficient matrix operator and the transmission coefficient matrix operator, respectively.  $\mathbf{X}_+^{(n)}$  and  $\mathbf{X}_-^{(n)}$  are the  $M^+ \times M^+$  diagonal matrix of the exponential term of the positive mode,  $\exp[-j(qG_z + k_z^{(g+)})d]$ , and the  $M^- \times M^-$  diagonal matrix of the exponential term of the negative mode,  $\exp[-j(qG_z + k_z^{(g-)})d]$ , respectively.

The coupling coefficient matrix operators  $\mathbf{C}_a^{(n,n)+}$ ,  $\mathbf{C}_a^{(n,n)-}$  and the reflection and transmission operators  $\tilde{\mathbf{R}}^{(n,n)}$  and  $\tilde{\mathbf{T}}^{(n,n)}$  of the left-to-right characterization are obtained, respectively, from Eqs. (20a) and (20b), as

layer and the  $(n+1)$ th layer. The reflection and transmission matrix operators,  $\tilde{\mathbf{R}}^{(n,n+1)}$ ,  $\tilde{\mathbf{T}}^{(n,n+1)}$ ,  $\tilde{\mathbf{R}}^{(n+1,n)}$ , and  $\tilde{\mathbf{T}}^{(n+1,n)}$  are obtained by Redheffer's star product relation:

$$\begin{aligned} \tilde{\mathbf{R}}^{(n,n+1)} &= \tilde{\mathbf{R}}^{(n,n)} + \tilde{\mathbf{T}}^{(n,n)} [(\mathbf{I} - \tilde{\mathbf{R}}^{(n+1,n+1)} \tilde{\mathbf{R}}^{(n,n)})^{-1}] \\ &\quad \times \tilde{\mathbf{R}}^{(n+1,n+1)} \tilde{\mathbf{T}}^{(n,n)}, \end{aligned} \quad (23a)$$

$$\tilde{\mathbf{T}}^{(n,n+1)} = \tilde{\mathbf{T}}^{(n+1,n+1)} [(\mathbf{I} - \tilde{\mathbf{R}}^{(n,n)} \tilde{\mathbf{R}}^{(n+1,n+1)})^{-1}] \tilde{\mathbf{T}}^{(n,n)}, \quad (23b)$$

$$\begin{aligned} \tilde{\mathbf{R}}^{(n+1,n)} &= \tilde{\mathbf{R}}^{(n+1,n+1)} + \tilde{\mathbf{T}}^{(n+1,n+1)} [(\mathbf{I} - \tilde{\mathbf{R}}^{(n,n)} \tilde{\mathbf{R}}^{(n+1,n+1)})^{-1}] \\ &\quad \times \tilde{\mathbf{R}}^{(n,n)} \tilde{\mathbf{T}}^{(n+1,n+1)}, \end{aligned} \quad (23c)$$

$$\tilde{\mathbf{T}}^{(n+1,n)} = \tilde{\mathbf{T}}^{(n,n)} [(\mathbf{I} - \tilde{\mathbf{R}}^{(n+1,n+1)} \tilde{\mathbf{R}}^{(n,n)})^{-1}] \tilde{\mathbf{T}}^{(n+1,n+1)}. \quad (23d)$$

Let us denote the internal coupling coefficient operators of the combined multilayer  $\mathbf{C}_a^{(n,n+1)}$  and  $\mathbf{C}_b^{(n,n+1)}$ .  $\mathbf{C}_a^{(n,n+1)}$  and  $\mathbf{C}_b^{(n,n+1)}$  are  $[4(2H+1)] \times [8(2H+1)]$  matrices given by

$$\mathbf{C}_a^{(n,n+1)} = (\mathbf{C}_{a,1}^{(n,n+1)} \quad \mathbf{C}_{a,2}^{(n,n+1)}), \quad (24a)$$

$$\mathbf{C}_b^{(n,n+1)} = (\mathbf{C}_{b,1}^{(n,n+1)} \quad \mathbf{C}_{b,2}^{(n,n+1)}), \quad (24b)$$

where  $(\mathbf{C}_{a,1}^{(n,n+1)}, \mathbf{C}_{b,1}^{(n,n+1)})$  and  $(\mathbf{C}_{a,2}^{(n,n+1)}, \mathbf{C}_{b,2}^{(n,n+1)})$  are the re-

spective coupling coefficient matrix operators corresponding to the  $n$ th layer and the  $(n+1)$ th layer. Then the formulas of the internal coupling coefficients are given as

$$\begin{pmatrix} \mathbf{C}_{a,1}^{(n,n+1)} \\ \mathbf{C}_{b,1}^{(n,n+1)} \end{pmatrix} = \begin{pmatrix} \mathbf{C}_a^{(n,n)} + \mathbf{C}_b^{(n,n)}(\mathbf{I} - \tilde{\mathbf{R}}^{(n+1,n+1)}\tilde{\mathbf{R}}^{(n,n)})^{-1}\tilde{\mathbf{R}}^{(n+1,n+1)}\tilde{\mathbf{T}}^{(n,n)} \\ \mathbf{C}_b^{(n,n)}(\mathbf{I} - \tilde{\mathbf{R}}^{(n+1,n+1)}\tilde{\mathbf{R}}^{(n,n)})^{-1}\tilde{\mathbf{T}}^{(n+1,n+1)} \end{pmatrix}, \quad (25a)$$

$$\begin{pmatrix} \mathbf{C}_{a,2}^{(n,n+1)} \\ \mathbf{C}_{b,2}^{(n,n+1)} \end{pmatrix} = \begin{pmatrix} \mathbf{C}_a^{(n+1,n+1)}(\mathbf{I} - \tilde{\mathbf{R}}^{(n,n)}\tilde{\mathbf{R}}^{(n+1,n+1)})^{-1}\tilde{\mathbf{T}}^{(n,n)} \\ \mathbf{C}_b^{(n+1,n+1)} + \mathbf{C}_a^{(n+1,n+1)}(\mathbf{I} - \tilde{\mathbf{R}}^{(n,n)}\tilde{\mathbf{R}}^{(n+1,n+1)})^{-1}\tilde{\mathbf{R}}^{(n,n)}\tilde{\mathbf{T}}^{(n+1,n+1)} \end{pmatrix}. \quad (25b)$$

The relationship can be referred to as the extended Redheffer's star product and denoted by the form

$$\begin{pmatrix} \mathbf{C}_a^{(n,n+1)} & \mathbf{C}_b^{(n,n+1)} \\ \mathbf{C}_a^{(n,n)} & \mathbf{C}_b^{(n,n)} \end{pmatrix} = \begin{pmatrix} \mathbf{C}_a^{(n+1,n+1)} & \mathbf{C}_b^{(n+1,n+1)} \\ \mathbf{C}_a^{(n,n)} & \mathbf{C}_b^{(n,n)} \end{pmatrix} * \begin{pmatrix} \mathbf{C}_a^{(n,n+1)} & \mathbf{C}_b^{(n,n+1)} \\ \mathbf{C}_a^{(n+1,n+1)} & \mathbf{C}_b^{(n+1,n+1)} \end{pmatrix}. \quad (26)$$

#### 4. NUMERICAL RESULTS AND DISCUSSION

In this section, some numerical results obtained by the proposed PFMA scheme will be presented. With comparison of the results obtained by the proposed PFMA and the conventional RCWA, the limitation of the conventional RCWA using the staircase approximation will be manifested, and the validity and correctness of the proposed scheme will be proved. Since it is well known that errors induced by the staircase approximation are significant for metallic structures, subwavelength metallic triangle grating structures are selected as example target structures to be analyzed. It can be expected that the continuous modeling of target structures without the staircase approximation produces more accurate results than the conventional method.

Figure 6 shows a subwavelength metallic triangle grating structure with base length of 211 nm, height of 35.2 nm, and period,  $T_x$ , of 316.6 nm. The permittivity values of the surrounding medium and the grating material are set to 1 and  $-10.1592 + j0.8294$ , respectively. In the RCWA, a multilayer with 30 layers is adopted in approximating the triangle structure. On the other hand, in the PFMA, just one triangle layer is used. In other words, in the PFMA, the whole triangle structure is represented by

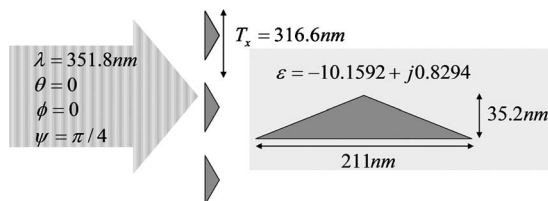


Fig. 6. Subwavelength metallic triangle grating structure.

a 2-D Fourier series without the multilayer modeling. The analytic Fourier transform of a trapezoid is given in Appendix A. In the analysis, a plane wave of wavelength 351.8 nm is normally incident on the grating structure, as shown in Fig. 6. In Fig. 7, the electric field distributions obtained by the RCWA and the PFMA are compared. In the simulation, the  $x$ -direction Fourier truncation order  $H$  is set to 14, and in the PFMA, the  $z$ -direction Fourier truncation order  $Q$  is set to 8. In Figs. 7(a) and 7(b), the  $y$ -direction electric field distributions,  $|E_y|$ , i.e., TE field distributions obtained by the PFMA and the RCWA respectively, are shown. We cannot see any significant differences between the two figures.

However, in the case of the  $x$ -direction electric field,  $|E_x|$ , and the  $z$ -direction electric field,  $|E_z|$ , significant differences appear, as seen in Figs. 7(c) and 7(d) and Figs. 7(e) and 7(f), respectively. It is observed that around the metal grating surface, the  $z$ -direction electric field,  $|E_z|$ , exists as shown in Figs. 7(e) and 7(g). However, in the case of the RCWA, nonphysical high electric field peaks are observed on the grating surface as indicated in Figs. 7(f) and 7(h). This kind of nonphysical high peak was also reported and discussed in Ref. [12].

Let us observe these inherent structural errors introduced by the staircase approximation in detail. In Fig. 8, another metallic triangle grating structure is shown with base length of 211 nm, height of 176 nm, and period,  $T_x$ , of 316 nm. The permittivity value of the grating material is  $-10.1592 + j0.8294$ . To allow observation of the effect of the staircase approximation, the RCWA on this grating structure is repeated with several staircase levels. The obtained  $z$ -direction electric field distributions are presented in Fig. 9. We can observe some digitized errors and high-intensity peak patterns in the  $z$ -direction electric field distributions,  $|E_z|$ , of each staircase level and that the error pattern seems to converge at a level number higher than 64. Therefore, we can see that the observed high peaks shown in Fig. 7(h) originate from the staircase approximation of the smooth triangle profile.

Next, the numerical results of the PFMA on the grating structure shown in Fig. 8 are compared with those of the RCWA. In the PFMA, the grating structure is modeled by a multilayer with 30 layers, as shown in Fig. 4(a). Two cases of normal incidence and 45-deg oblique incidence

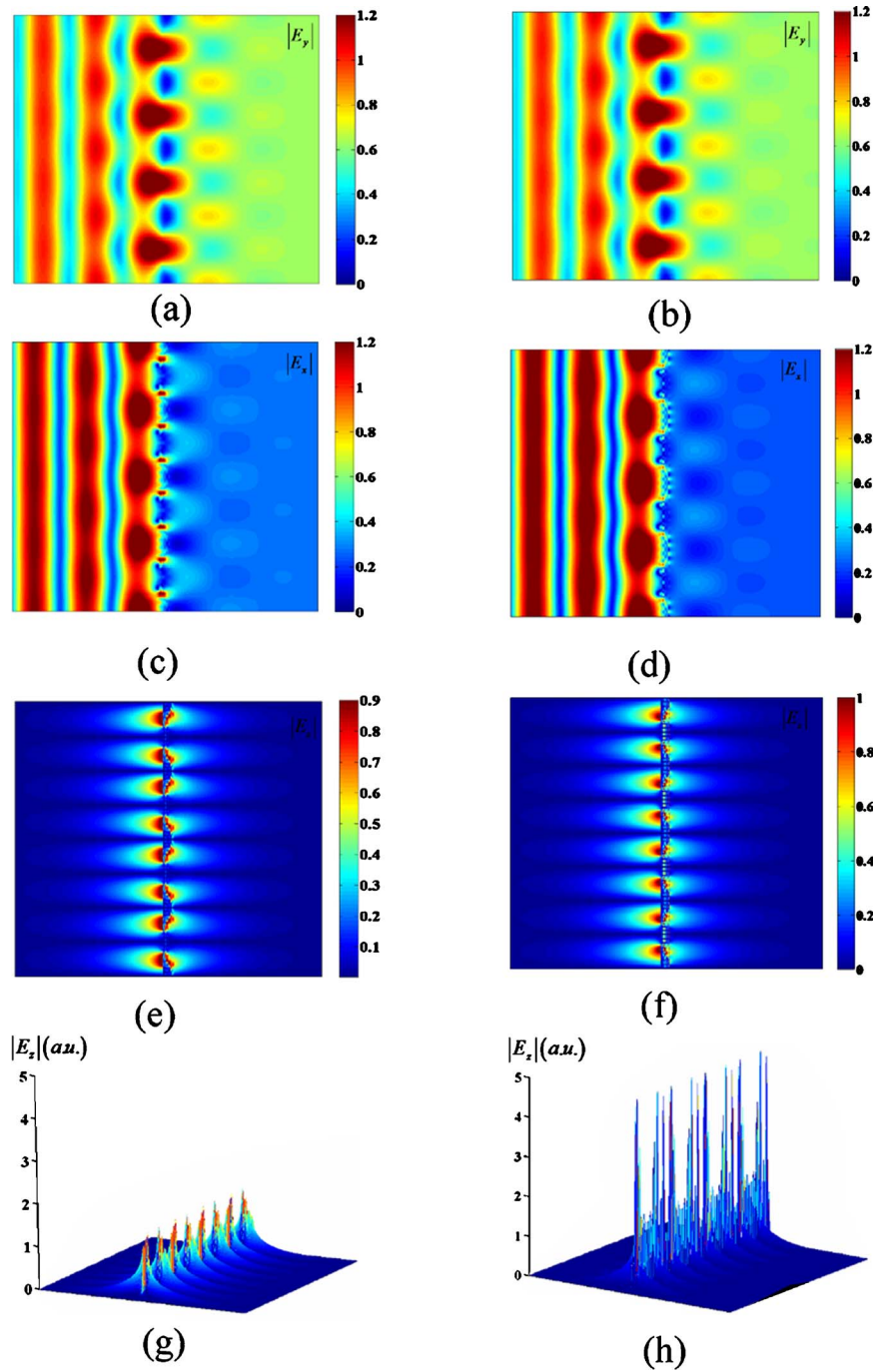


Fig. 7. (Color online) Comparison of the PFMA and the RCWA simulation results: (a)  $|E_y|$  obtained by the PFMA, (b)  $|E_y|$  obtained by the RCWA, (c)  $|E_x|$  obtained by the PFMA, (d)  $|E_x|$  obtained by the RCWA, (e)  $|E_z|$  obtained by the PFMA, (f)  $|E_z|$  obtained by the RCWA, (g)  $|E_z|$  obtained by the PFMA, (h)  $|E_z|$  obtained by the RCWA.

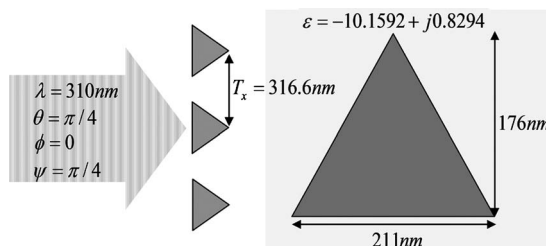


Fig. 8. Subwavelength metallic triangle grating structure.

are considered for proving the advantages of the PFMA over the RCWA. In Fig. 10, the electric field distributions obtained in the case of oblique incidence are presented. In Figs. 10(a) and 10(b), the  $y$ -direction electric field distributions,  $|E_y|$ , obtained by the PFMA and the RCWA, respectively, are shown. As in the case of the previous example, no significant differences appear in the two figures. However, in the case of the TM field—that is, the  $x$ -direction electric field,  $|E_x|$ , and the  $z$ -direction electric field,  $|E_z|$ —comparing the results of the PFMA shown in

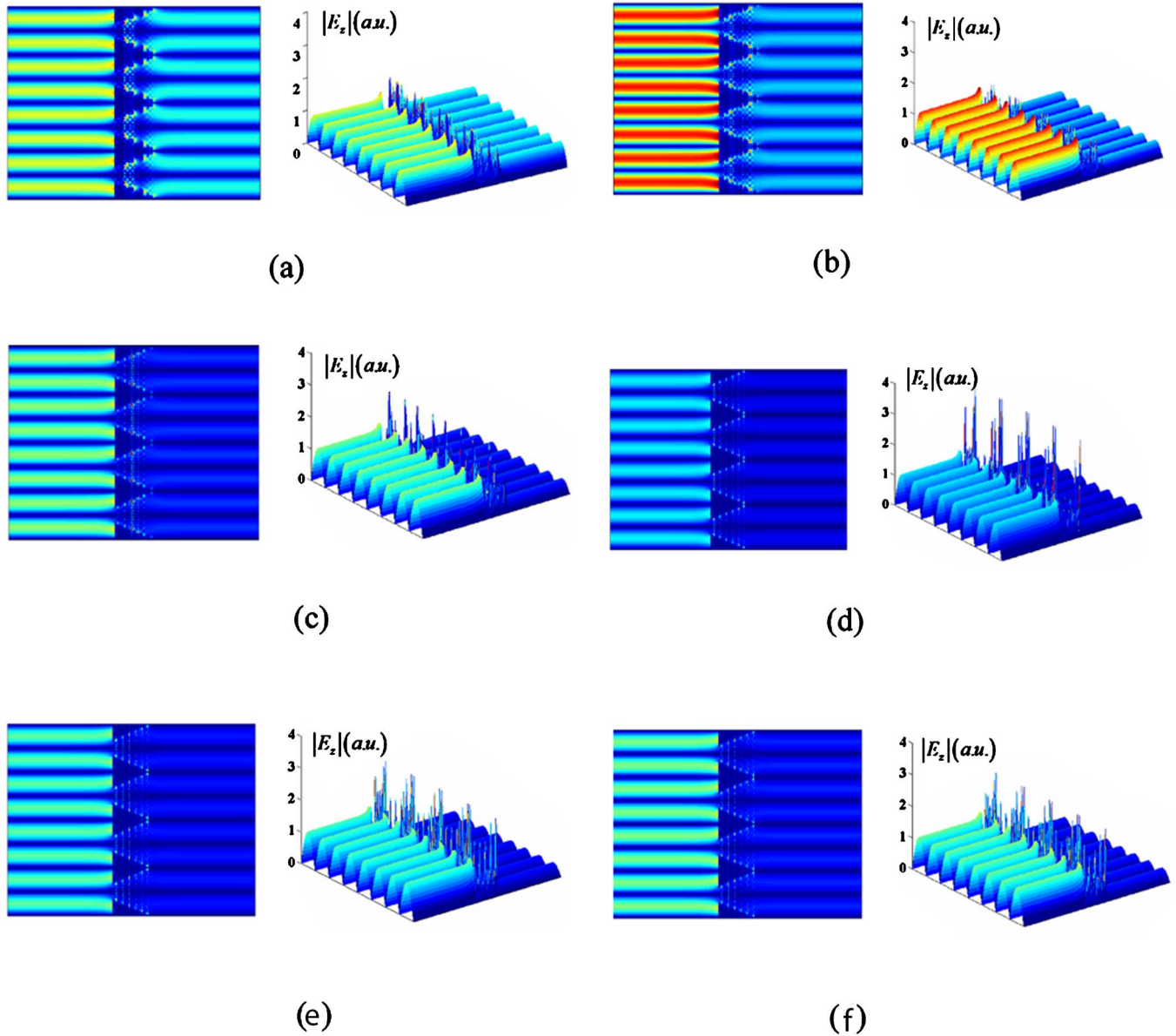


Fig. 9. (Color online)  $z$ -direction electric field distribution,  $|E_z|$ , obtained by the RCWA with the staircase approximation of (a) 4 levels, (b) 8 levels, (c) 16 levels, (d) 32 levels, (e) 64 levels, and (f) 128 levels.

Figs. 10(c) and 10(e) and those of the RCWA shown in Figs. 10(d) and 10(f), we can perceive significant differences in the field distribution. Nonphysical discontinuous field distributions that might not naturally exist around the smooth metal grating surface are observed in Figs. 10(d) and 10(f). These unnatural field distributions observed in the RCWA results originate from the improper staircase approximation of the smooth metallic structure. In Fig. 11, a comparison of the PFMA and the RCWA in the case of normal incidence is presented. Just as in the case of oblique incidence, in the case of normal incidence the limitation of the RCWA with the staircase approximation can be observed, while the PFMA shows natural field distributions.

In fact, the field distributions presented here cannot be said to be convergent enough. Convergence is difficult to

attain in practice in the PFMA because of the degeneracy problem. With use of a personal computer, the number of truncation orders retained in computation is seriously limited. Although the increase in truncation orders may be possible with use of parallel computers, this study is considered as research independent of the parallel implementation of the FMM. Definitely, as the truncation order increases, the PFMA will converge at a certain level, although the task requires large-scale parallel computation. In this paper, we discussed the full-frequency formalism, PFMA, and the effect of the staircase approximation within the FMM framework by comparing the PFMA and the RCWA. We can perceive and understand the difference between the RCWA and the PFMA, although the field distributions may not be completely converged.

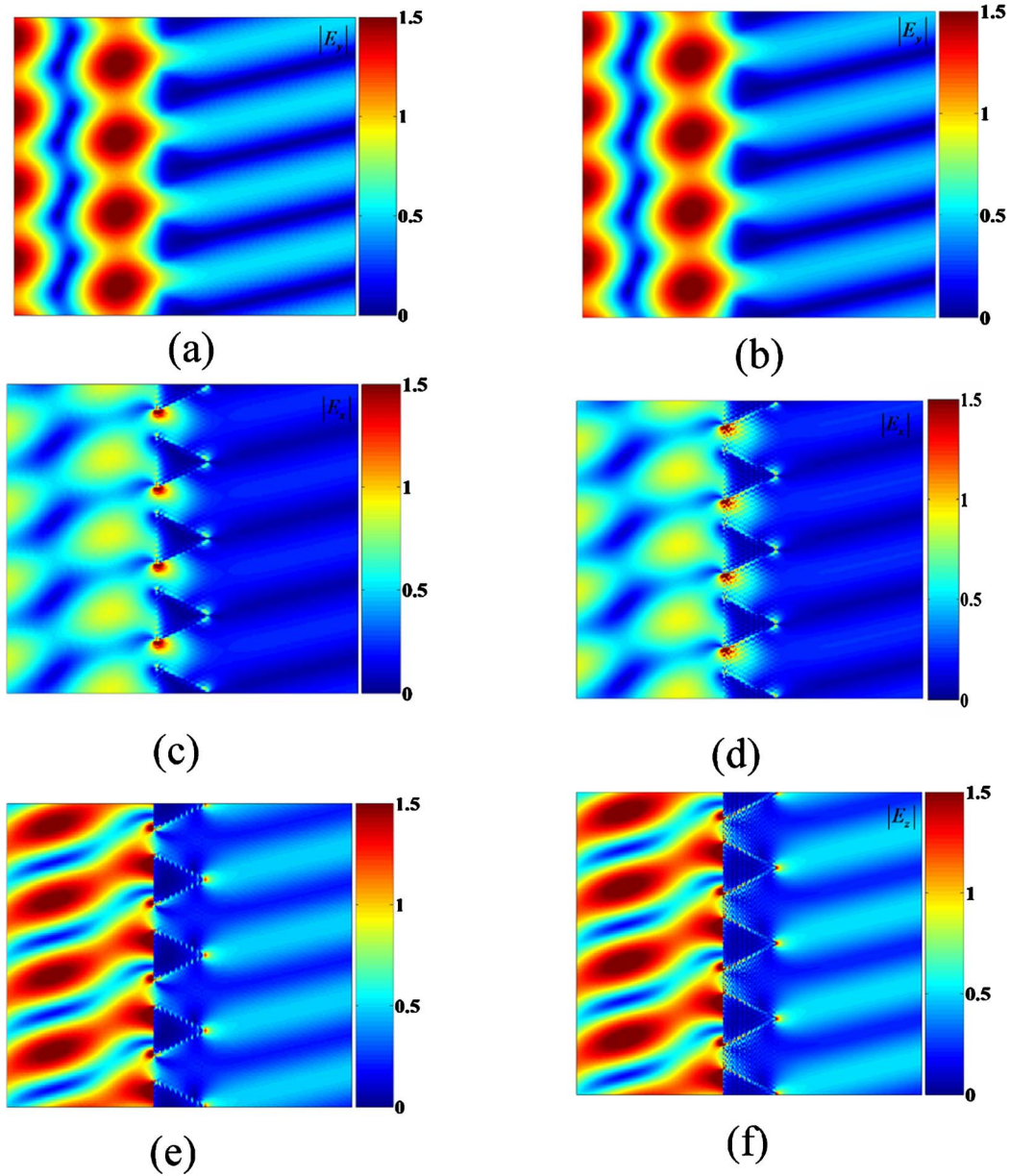


Fig. 10. (Color online) Oblique incidence: (a)  $|E_y|$  obtained by the PFMA, (b)  $|E_y|$  obtained by the RCWA, (c)  $|E_x|$  obtained by the PFMA, (d)  $|E_x|$  obtained by the RCWA, (e)  $|E_z|$  obtained by the PFMA, (f)  $|E_z|$  obtained by the RCWA.

## 5. CONCLUSION

In this paper, the general scheme of the PFMA with the ESMM for modeling 2-D arbitrarily shaped grating structures has been described. Arbitrarily shaped metallic grating structures are modeled by multilayer structures without the staircase approximation, based on 2-D Fourier representation of the structures. It has been shown that this method can eliminate the inherent errors of the staircase approximation in the analysis of metallic grating structures. The PFMA can be widely applied in optics and photonics. It is expected that the described scheme will be particularly useful for the modeling and simulation of phenomena, devices, and systems in the field of

plasmonics on a subwavelength scale that studies mainly metallic structures.

## APPENDIX A

Figure 12 shows a trapezoid Fourier transform of a trapezoid. Let the trapezoid function  $\Gamma(x,y)$  be defined by

$$\Gamma(x,y) = \begin{cases} 1 & \text{for } (x,y) \in \text{trapezoid} \\ 0 & \text{for } (x,y) \notin \text{trapezoid} \end{cases} \quad (\text{A1})$$

The 2-D Fourier transform of this trapezoid function,  $F(f_x, f_y)$ , is obtained by

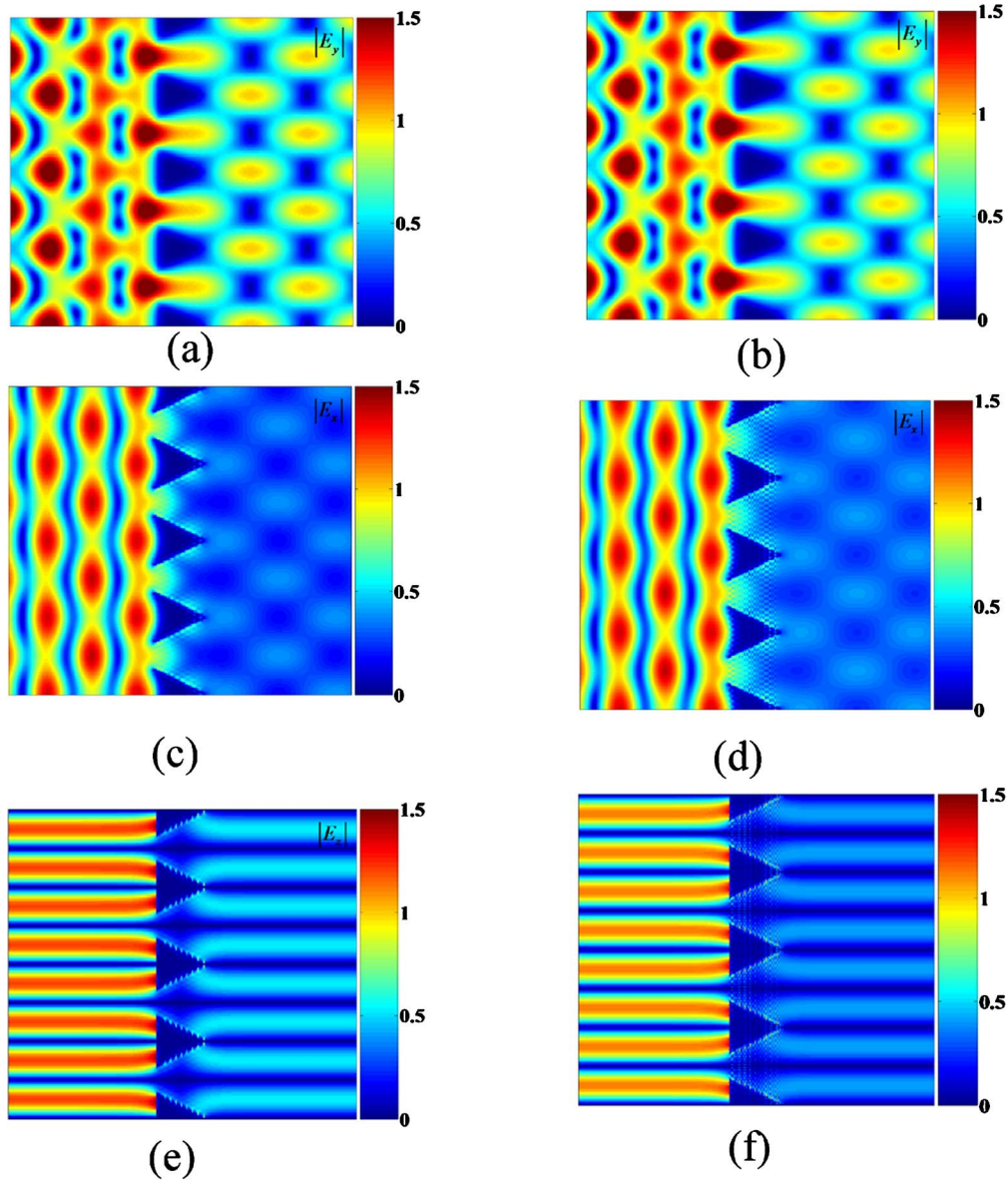


Fig. 11. (Color online) Normal incidence: (a)  $|E_y|$  obtained by the PFMA, (b)  $|E_y|$  obtained by the RCWA, (c)  $|E_x|$  obtained by the PFMA, (d)  $|E_x|$  obtained by the RCWA, (e)  $|E_z|$  obtained by the PFMA, (f)  $|E_z|$  obtained by the RCWA.

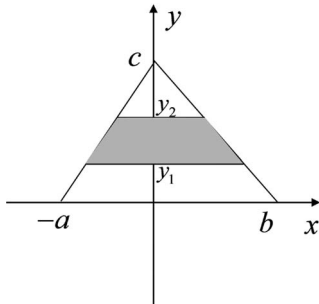


Fig. 12. Trapezoid.

$$\begin{aligned}
 & \text{for } f_x \neq 0 \text{ and } f_y \neq 0, \\
 F(f_x, f_y) &= \left( \frac{-j(y_2 - y_1)}{2\pi f_x} \right) \\
 & \times \left\{ \begin{aligned} & -e^{-2\pi f_x b} e^{j2\pi \left(\frac{f_x b}{c} - f_y\right) \left(\frac{y_1 + y_2}{2}\right)} \text{sinc} \left[ \left(\frac{f_x b}{c} - f_y\right) (y_2 - y_1) \right] \\ & + e^{-2\pi f_x a} e^{-j2\pi \left(\frac{f_x a}{c} + f_y\right) \left(\frac{y_1 + y_2}{2}\right)} \text{sinc} \left[ \left(\frac{f_x a}{c} + f_y\right) (y_2 - y_1) \right] \end{aligned} \right\}; \tag{A2}
 \end{aligned}$$

for  $f_x = 0$  and  $f_y \neq 0$ ,

$$F(f_x, f_y) = \left( \frac{a + b}{c} \right) e^{-i2\pi f_y c} \left\{ \frac{[j2\pi(c - y_2)f_y - 1]e^{j2\pi f_y(c - y_2)} - [j2\pi(c - y_1)f_y - 1]e^{j2\pi f_y(c - y_1)}}{(2\pi f_y)^2} \right\}; \tag{A3}$$

for  $f_x=0$  and  $f_y=0$ ,

$$F_{f_x f_y} = \left\{ \frac{(a+b)(y_2-y_1)(2c-y_1-y_2)}{2c} \right\}. \quad (\text{A4})$$

## ACKNOWLEDGMENTS

The authors acknowledge the support by the Ministry of Science and Technology of Korea and the Korea Science and Engineering Foundation through the Creative Research Initiative Program (Active Plasmonics Applications Systems).

## REFERENCES

1. M. G. Moharam and T. K. Gaylord, "Rigorous coupled-wave analysis of planar-grating diffraction," *J. Opt. Soc. Am.* **71**, 811–818 (1981).
2. P. Lalanne, "Improved formulation of the coupled-wave method for two-dimensional gratings," *J. Opt. Soc. Am. A* **14**, 1592–1598 (1997).
3. L. Li, "Use of Fourier series in the analysis of discontinuous periodic structures," *J. Opt. Soc. Am. A* **13**, 1870–1876 (1996).
4. L. Li, "Fourier modal method for crossed anisotropic gratings with arbitrary permittivity and permeability tensors," *J. Opt. A, Pure Appl. Opt.* **5**, 345–355 (2003).
5. L. Li, "Mathematical reflections on the Fourier modal method in grating theory," in *Mathematical Modeling in Optical Science*, G. Bao, ed. (SIAM, 2001), Chap. 4.
6. E. Popov and M. Nevière, "Differential theory for diffraction gratings: a new formulation for TM polarization with rapid convergence," *Opt. Lett.* **25**, 598–600 (2000).
7. E. Popov and M. Nevière, "Grating theory: new equations in Fourier space leading to fast converging results for TM polarization," *J. Opt. Soc. Am. A* **17**, 1773–1784 (2000).
8. J. P. Hugonin and P. Lalanne, "Perfectly matched layers as nonlinear coordinate transforms: a generalized formalization," *J. Opt. Soc. Am. A* **22**, 1844–1849 (2005).
9. L. Li, "Formulation and comparison of two recursive matrix algorithms for modeling layered diffraction gratings," *J. Opt. Soc. Am. A* **13**, 1024–1035 (1996).
10. H. Kim, I.-M. Lee, and B. Lee, "Extended scattering matrix method for efficient full parallel implementation of rigorous coupled wave analysis," *J. Opt. Soc. Am. A* **24**, 2313–2327 (2007).
11. E. Popov, M. Nevière, B. Gralak, and G. Tayeb, "Staircase approximation validity for arbitrary-shaped gratings," *J. Opt. Soc. Am. A* **19**, 33–42 (2002).
12. W. Jiang and R. T. Chen, "Rigorous analysis of diffraction gratings of arbitrary profiles using virtual photonic crystals," *J. Opt. Soc. Am. A* **23**, 2192–2197 (2006).
13. H. Kim, S. Kim, I.-M. Lee, and B. Lee, "Pseudo-Fourier modal analysis on dielectric slabs with arbitrary longitudinal permittivity and permeability profiles," *J. Opt. Soc. Am. A* **23**, 2177–2191 (2006).
14. K. Mehrany and B. Rashidian, "Polynomial expansion of electromagnetic eigenmodes in layered structures," *J. Opt. Soc. Am. B* **20**, 2434–2441 (2003).
15. M. Chamanzar, K. Mehrany, and B. Rashidian, "Legendre polynomial expansion for analysis of linear one-dimensional inhomogeneous optical structures and photonic crystals," *J. Opt. Soc. Am. B* **23**, 969–977 (2006).
16. M. Chamanzar, K. Mehrany, and B. Rashidian, "Planar diffraction analysis of homogeneous and longitudinally inhomogeneous gratings based on Legendre expansion of electromagnetic fields," *IEEE Trans. Antennas Propag.* **54**, 3686–3694 (2006).